PERGAMON

Journal of Structural Geology 21 (1999) 795–806

JOURNAL OF STRUCTURAL GEOLOGY

Permeability anisotropy and pressure dependency of permeability in experimentally sheared gouge materials

Shuqing Zhang*,[1], Terry E. Tullis, Valerie J. Scruggs

Department of Geological Sciences, Brown University, Providence, RI 02912 USA

Received 17 February 1998; accepted 10 March 1999

Abstract

The effects of fault slip and effective mean stress on permeability and permeability anisotropy have been investigated during long displacement shearing of synthetic quartz, feldspar, muscovite and granitic gouges under high pressures. In quartzo-feldspathic gouges, permeability anisotropies up to one-and-a-half orders of magnitude were developed by heterogeneous grain crushing associated with shear sliding. In muscovite gouge, a permeability anisotropy of about one order of magnitude was first developed during initial pressurization of gouge materials due to a preferred alignment of mica basal planes. During shear sliding, rearrangement of packing and rotation of mica basal planes lead to a slight decrease in permeability anisotropy. The pressure dependency of permeability of gouge materials changes systematically with shear displacements. In quartzo-feldspathic gouges, the pressure dependency of permeability first decreased with shear sliding and then increased to a value typical for rocks containing microcracks. In contrast, the pressure dependency of permeability in muscovite gouge decreases continuously with increasing shear displacement.

The evolution of permeability anisotropy and pressure dependency of permeability for different gouge materials during shear sliding implies that the distribution of fluid pressure in natural fault zones could be very heterogeneous.

1. Introduction

Brittle fault zones in the Earth's crust are distinct structural components in which fluid flow and fluid pressure distribution may be markedly different from outside of the fault zones (Brace, 1980; Ganser, 1987; Bruhn et al., 1990; Byerlee, 1990, 1993; Moore and Vrolijk, 1992; Rice, 1992; Sleep and Blanpied, 1992). It has long been known that fault zones performed two seemingly contradictory roles: that of barrier to fluid flow, and that of conduit (Hubbert, 1953; Davis and DeWiest, 1966; Smith, 1966, 1980; Levorsen, 1967; Sibson, 1981; Powley, 1990; Hippler, 1993). Individual faults may also exhibit both high and low permeabilities, with high permeability parallel to the fault plane, and low permeability perpendicular to the fault plane (Seeburger, 1981; Arch and Maltman, 1990; Rice, 1992; Antonellini and Aydin, 1994; Scholz and Anders, 1994). The observed permeability anisotropy implies that the fault zone itself is structurally anisotropic.

Studies on the internal structure of natural fault zones reveal that fault zones are usually composed of a fault core where most of the displacement is accommodated and a surrounding fractured/damaged zone that is mechanically related to the growth of the fault zone (Sibson, 1977; Chester and Logan, 1986; Chester et al., 1993; Scholz and Anders, 1994; Caine et al., 1996; Evans et al., 1997). The thickness, distribution, and permeability of the fault core relative to its surrounding damaged zone as well as the anisotropic structures within each component determine fluid flow and fluid pressure distribution within the fault zones (Scholz and Anders, 1994; Caine et al., 1996; Zhang and Tullis, 1998).

* Corresponding author.
E-mail address: shuqing.zhang@anu.edu.au (S. Zhang)
[1] Now at Research School of Earth Sciences, The Australian National University, Canberra, ACT 0200, Australia.

0191-8141/99/$ - see front matter
PII: S0191-8141(99)00080-2

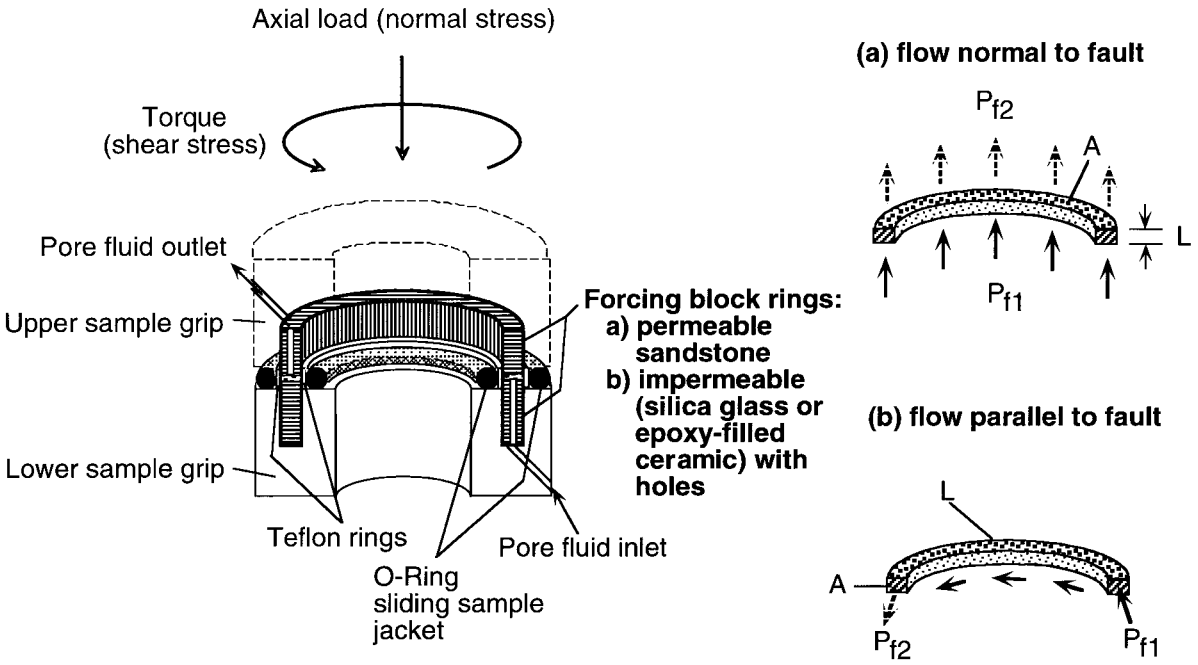

Fig. 1. An illustration of half of the specimen assembly for rotary shear deformation. An experimental fault with or without artificial gouge lies between the upper and lower forcing block rings. The pore fluid pressure system is separated from the confining pressure system by two teflon rings and two O-rings outside and inside of the forcing block rings. Fluid permeability perpendicular and parallel to the fault is measured with permeable and impermeable forcing blocks, respectively. The flow direction (arrows), area (A), path length (L), and inlet and outlet pore pressures (P_{f1} and P_{f2}) for permeability measurements are shown in (a) and (b).

In exhumed fault zones, the fault cores are usually composed of well-defined, narrow layers of coarse breccia, finely milled rock flour (gouge) or chemically altered and highly indurated cataclasite (Sibson, 1977; Anderson et al., 1983; Chester and Logan, 1986). The fault cores have distinctive internal shear textures such as Riedel shears, P-shears and Y-shears, which are well-reproduced in frictional sliding experiments (Logan et al., 1979; Rutter et al., 1986). It has been suggested that grain-size reduction and chemical alteration are the two key factors affecting fluid permeability of fault cores (Pittman, 1981; Seeburger, 1981; Caine et al., 1996) and that the shear textures may lead to anisotropic fluid flow in fault zones (Mandl et al., 1977). Previous frictional sliding experiments showed that the evolution of shear textures in fault gouges is largely a function of cumulative slip displacement (Mandl ey al., 1977; Logan et al., 1992; Gu and Wong, 1994; Scruggs and Tullis, 1995). At small shear displacements, deformation is usually accommodated by anastomosing Riedel shears and P-shears; whereas at large displacements, deformation tends to localize along shear-plane-parallel Y-shears. As a result, the permeability anisotropy may depend strongly on shear displacement if these shear textures are important for fluid flow.

Bearing in mind the lack of quantitative measurements of permeability anisotropy in fault products, we have developed a novel technique for laboratory measurements of permeabilities both perpendicular and parallel to an experimental fault during large displacement frictional sliding. In an earlier study, we measured the permeability anisotropy during large displacement shearing of quartz gouge at a normal stress of 25 MPa; we correlated the development of permeability anisotropy with shear localization along Y-shears (Zhang and Tullis, 1998). Since then, we have extended our measurements to other major mineral components in the Earth's upper crust including feldspar, biotite, muscovite and granitic gouge. In most of those later experiments, we sheared the gouge materials under a normal stress of 100 MPa and intermittently cycled pore fluid pressure in the same specimens sheared to different displacements. These exploratory experiments now allow us to generalize the effects of shear displacement, sliding velocity, mineral compositions, and effective mean stress on permeability and permeability anisotropy. In this paper, we will first demonstrate the large differences between quartzofeldspathic gouges and mica gouges in terms of the evolution of permeability and permeability anisotropy; we will then discuss their implications for fluid flow and pore fluid pressure distribution within natural fault zones.

Table 1
Typical sequence of pressure cycling for determining pressure dependency of permeability

Steps	P_c (MPa)	P_f (MPa)	σ_a (MPa)	σ_n (MPa)	σ_m (MPa)
		During initial pressurization			
1	25.0	4.0	4.0	25.0	22.3
2	50.0	8.0	8.0	50.0	44.7
3	75.0	12.0	12.0	75.0	67.0
4	100.0	16.0	16.0	100.0	89.3
		During shear deformation[a]			
1	100.0	16.0	16.0	100.0	89.3
2	86.4	16.0	13.6	85.0	75.9
3	75.0	16.0	11.2	70.0	62.5
4	74.8	28.6	8.8	55.0	49.1
5	74.8	41.2	6.4	40.0	35.7
6	74.8	53.8	4.0	25.0	22.3
7	74.8	41.2	6.4	40.0	35.7
8	74.8	28.6	8.8	55.0	49.1
9	74.8	16.0	11.2	70.0	62.5
10	100.0	16.0	4.0	100.0	89.3

[a] Similar steps of cycling effective normal stress (σ_n) were conducted at shear displacement of 5, 15, 50, and 100 mm. Fluid permeability was measured at each step. P_c, P_f, σ_a, and σ_m are the confining pressure, pore fluid pressure, axial stress, and the effective mean stress, respectively.

2. Experimental set-up

Pure quartz, feldspar, and mica gouges were prepared by mechanically crushing silica sand, Tanco Albite, and separated mica aggregates, respectively. The granitic gouge is ground Westerly granite which has a modal mineral composition of 35% microcline, 32% plagioclase, 28% quartz, 5% mica and $<1\%$ magnetite (Brace et al., 1965). All gouge powders were sieved through a #170 mesh (<88 μm). The initial particle size distribution of gouge materials was examined in thin section by light microscopy. In quartz gouge, more than 90% particles have diameters between 50 and 88 μm. In both pure feldspar and granitic gouges, more than 60% particles are smaller than 25 μm and about 30% between 25 and 75 μm. In muscovite gouge, most flakes are 5–15 μm in width and 25–75 μm in length.

Frictional sliding experiments were done in a high pressure, computer-interfaced rotary shear apparatus (Tullis and Weeks, 1986; Beeler et al., 1996). Shear deformation occurs between the ends of two forcing block cylindrical rings which have an outer diameter of the sliding surface of 53.98 mm, an inner diameter of 44.45 mm, and an area of contact of 735 mm^2 (Fig. 1). The two forcing block rings are respectively attached to the upper and lower steel sample grips with epoxy. The upper sample grip is held fixed, and the lower grip is rotated around their common vertical axis by a steel piston. One revolution of lower grip rotation corresponds to a displacement of about 153.6 mm. An experimental fault zone is produced by placing an initial 1 mm thick layer of synthetic gouge materials between the two forcing block rings. Axial and rotary displacement are measured simultaneously with a LVDT transducer and a resolver, thus, allowing determination of changes in gouge layer thickness with shear displacement. All shear sliding experiments were conducted at an effective normal stress of 100 MPa which results from a combination of 100 MPa (N_2) gas confining pressure, 16 MPa pore fluid pressure and 16 MPa axial stress. Doubly deionized water was used as pore fluid. A sliding jacket assembly (Beeler et al., 1996) isolates the confining pressure gas from the pore fluid water. After intervals of displacement, the sliding was temporarily stopped, shear stress was removed, and the effective mean stress was changed in steps (Table 1) to investigate its influence on compaction–dilation and on permeability. The removal of shear stress is necessary for preventing shear sliding associated with reducing normal stress. As shown in Table 1, during pressure cycling, axial stress was changed in such a way that its ratio with effective pressure (confining pressure minus pore water pressure) remains about 4/21. This ratio of axial stress with effective pressure is necessary for preventing lateral extrusion of gouge materials. In the following sections, the effective normal stress is referred to as confining pressure minus pore water pressure plus axial stress. Step changes in sliding velocity were also made; most of the slip occurred at velocities of 1 and 10 μm/s.

Water flow through the gouge layer was maintained by two servo-controlled volumometers connected to the upper and lower sample grip, respectively. Each volumometer is composed of a piston-cylinder, a pressure transducer and a LVDT attached to the shaft of the volumometer piston. By respectively using the pore pressure and the LVDT signals as feedbacks, either pressure or flow rate can be servo-controlled independently for the ports into upper and lower sample grips. Fluid flow perpendicular to the gouge layer was achieved by using permeable ceramics as forcing block rings and by applying either a constant pressure difference or flow rate across the specimen (Fig. 1). Fluid flow parallel to the gouge layer was generated by introducing fluid to and away from the gouge layer via permeable slots at one or more locations around the circumference of the otherwise impermeable forcing block rings (epoxy-filled ceramics). Fluid permeability was calculated using Darcy's law. The calculation of the permeabilities for the gouge layer has taken into account the permeabilities of the forcing block rings or differences in fluid path lengths along the gouge layer as sliding occurs (Zhang and Tullis, 1998). The reproducibility for permeability measurements is within a factor of 1.2.

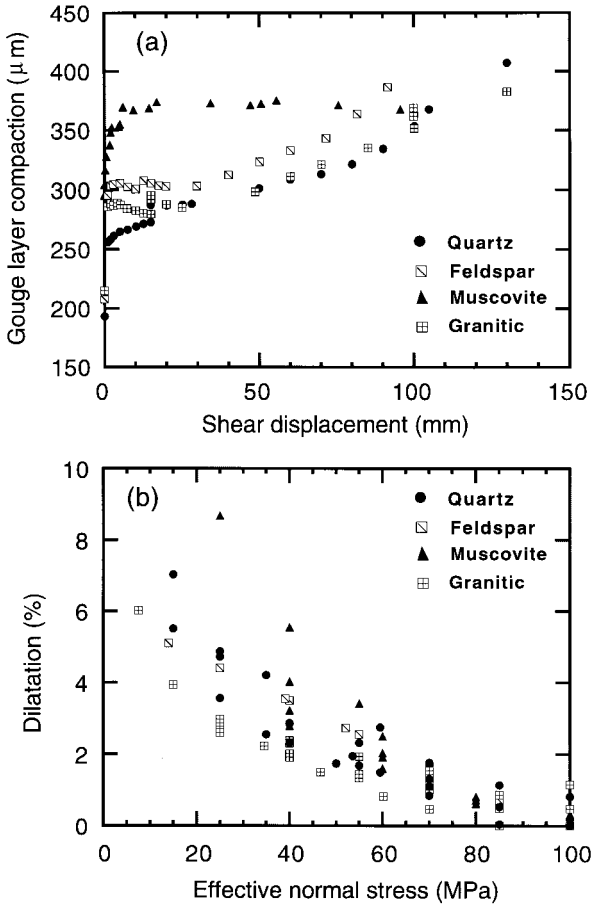

Fig. 2. Changes in gouge layer thickness. (a) Gouge layer compaction with shear displacement. The starting thickness for all gouge layers before pressurization is about 1 mm. During initial pressurization, thickness decreases with increasing pressure. The cumulative amount of gouge compaction after the effective normal stress reaches 100 MPa is shown at 0 mm shear displacement. (b) Gouge layer thickness increases with decreasing effective normal stress in sheared gouge. Dilatation is calculated as the change of gouge layer thickness associated with pore pressure cycling normalized by the gouge layer thickness at an effective normal stress of 100 MPa after shear sliding is halted. The variations of dilatation at the same effective normal stress for each gouge material are caused by differences in shear displacement. In general, dilatation decreases with increasing shear displacements.

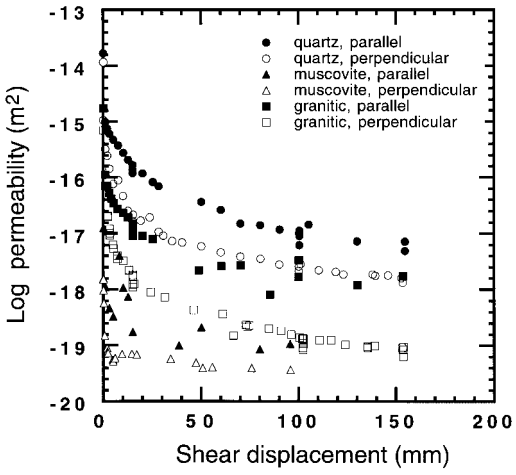

Fig. 3. Effect of shear sliding on permeability. Scattering of permeabilities at shear displacements of 15, 50, 100, and 150 mm is associated with effective stress cycling. In quartzo-feldspathic gouges, the permeability becomes lower after a complete stress cycling of first reducing effective mean stress to 22.3 MPa and then increasing back to 89.3 MPa, whereas in mica gouge, it becomes higher. Porosity and pore geometry must change during pore pressure cycling.

3. Experimental results

3.1. Changes in gouge thickness

During initial pressurization to a normal stress of 100 MPa, a relatively larger amount of compaction occurred in muscovite gouge than in quartzo-feldspathic gouges, whereas shear deformation-enhanced compaction was more effective in quartzo-feldspathic gouges than in muscovite gouge (Fig. 2a). During shear deformation, all gouge materials compacted sharply within the first 5 mm shear displacement or less. With further shear sliding, quartzo-feldspathic gouges compacted continuously, but at reduced rates. In contrast, further compaction in muscovite gouge was minimum and a small amount of dilatation occurred at a displacement larger than about 60 mm.

In gouge materials sheared 5–150 mm, decreases of effective normal stress from 100 to 15 MPa result in dilatations of about 6–9% (Fig. 2b). Muscovite gouge has somewhat larger amounts of dilatation than quartzo-feldspathic gouges. For quartzo-feldspathic materials, the amount of compaction associated with increasing effective normal stress back to 100 MPa is larger than the dilatation that occurred during the early stage of pore pressure increase. The gouge layer tends to dilate slightly during the initial part of the subsequent shear sliding. In contrast, muscovite gouge tends to have a larger amount of dilatation than compaction during a complete pore pressure cycle, and the gouge layer compacted initially during subsequent shearing.

3.2. Effect of fault slip on permeability anisotropy

At a constant normal stress, changes in permeability in sheared gouge materials are largely a function of shear displacement alone. Although a sliding velocity step is usually accompanied by transient dilatation or compaction, its effect on permeability is undetectable because of the overall trend of porosity reduction as indicated by the decreases in gouge layer thickness with shear sliding (Fig. 2a) and the small magnitude of dilatation or compaction (< 5 μm) for a typical 10-fold step in velocity within the range of velocities from 0.01 to 10 μm/s.

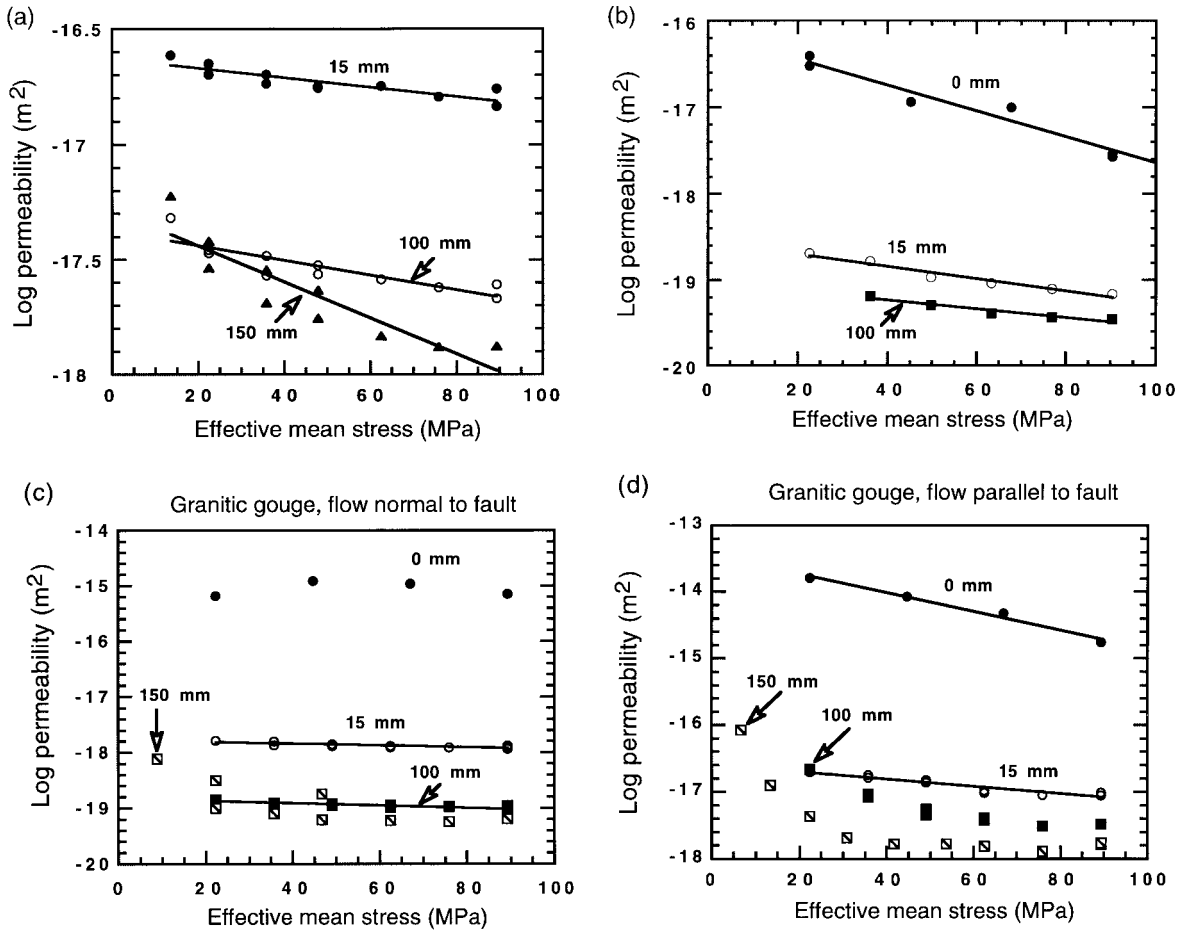

Fig. 4. Permeability as a function of effective mean stress in sheared gouge materials. The shear displacements prior to pore pressure cyclings are shown in each diagram. (a) Quartz gouge, fluid flow direction is perpendicular to the experimental fault plane; (b) muscovite gouge, fluid flow direction is perpendicular to the experimental fault plane; (c) granitic gouge, fluid flow direction is perpendicular to the experimental fault plane; and (d) granitic gouge, fluid flow direction is parallel to the experimental fault plane.

In quartzo-feldspathic gouges, permeability anisotropy is small during initial pressurization. Significant permeability anisotropies were developed after a few millimeters of shear sliding. In quartz gouge, the permeability is about 10^{-14} m^2 after applying an effective normal stress of 100 MPa. Shear deformation reduces the permeability more in the direction perpendicular to the fault than parallel to it. Up to a shear displacement of 150 mm, the permeability parallel to the fault is reduced by about three orders of magnitude, and that perpendicular to it by about four orders of magnitude (Fig. 3). The maximum permeability anisotropy is about one order of magnitude. In granitic gouge, the initial permeability is about 10^{-15} m^2 after pressurization to an effective normal stress of 100 MPa. Shear sliding up to a shear displacement of about 150 mm reduced fluid permeability by about three and four orders of magnitude in the directions parallel and perpendicular to the fault, respectively. Permeability anisotropy developed after about 5–10 mm shear displacement and it increased with increasing shear displacement. At a shear displacement of 150 mm, the permeability anisotropy is about one-and-a-half orders of magnitude.

In muscovite gouge, a permeability anisotropy was formed during initial packing and subsequent pressurization. Before shear deformation, the permeability parallel and perpendicular to the experimental fault were 10^{-17} and 10^{-18} m^2, respectively (Fig. 3). During shear deformation, permeabilities were reduced by between one and one-and-a-half orders of magnitude within the first 15 mm of shear displacement. The permeability decreases more in the direction parallel to the gouge layer than perpendicular to it, leading to a gradual decrease in permeability anisotropy. Further shear sliding led to only slight changes in permeability.

3.3. Pressure dependence of permeability

Following earlier work by Rice (1992) and David et al. (1994), we assume an exponential relationship between permeability (k) and effective mean stress (σ_m):

Table 2
Values of γ for gouge materials sheared to different displacements[a]

Shear displacement		0 mm	15 mm	50 mm	100 mm	150 mm
Quartz gouge	$k_\perp$	–	0.00472	–	0.00739	0.01801
Quartz gouge	$k_\parallel$	0.01417	0.00625	–	0.02057	0.02919
Muscovite gouge	$k_\perp$	0.01539	0.00626	0.00610	0.00376	–
Muscovite gouge	$k_\parallel$	0.01494	0.01172	0.01196	0.00796	–
Granitic gouge	$k_\perp$	–	0.00356	–	0.00476	*****
Granitic gouge	$k_\parallel$	0.03253	0.01248	–	*****	*****

[a] Values are MPa^{-1}. $k_\perp$ and $k_\parallel$ are the permeability perpendicular and parallel to the fault plane. – where either no measurement or value is not precisely determined. ***** where log permeability vs pressure is nonlinear.

$$k = k_0 \exp(-\gamma\sigma_m) \quad (1)$$

where k_0 is the permeability at zero effective mean stress and γ is the stress dependency of permeability. The effective mean stress (σ_m) is defined as $(\sigma_1 + 2\sigma_3)/3 - P_f$, where P_f is the pore fluid pressure, σ_1 and σ_3 are the maximum and the least principal stress, respectively. Because in most previous theoretical studies and laboratory measurements of permeability, hydrostatic loading path was used ($\sigma_m = \sigma_3 - P_f$), the value of γ has been commonly referred to as pressure dependency of permeability. In this paper, we will use this common terminology.

The fittings of Eq. (1) to our experimental data are shown as solid lines in Fig. 4. The derived values of γ for quartz, muscovite, and granitic gouges are listed in Table 2. The above empirical relation between permeability and the effective mean stress holds for all gouge materials during initial pressurization and for quartz and muscovite gouges sheared up to 150 mm (Fig. 4a and b). In granitic gouge sheared for more than 100 mm, log permeability is nonlinearly related to

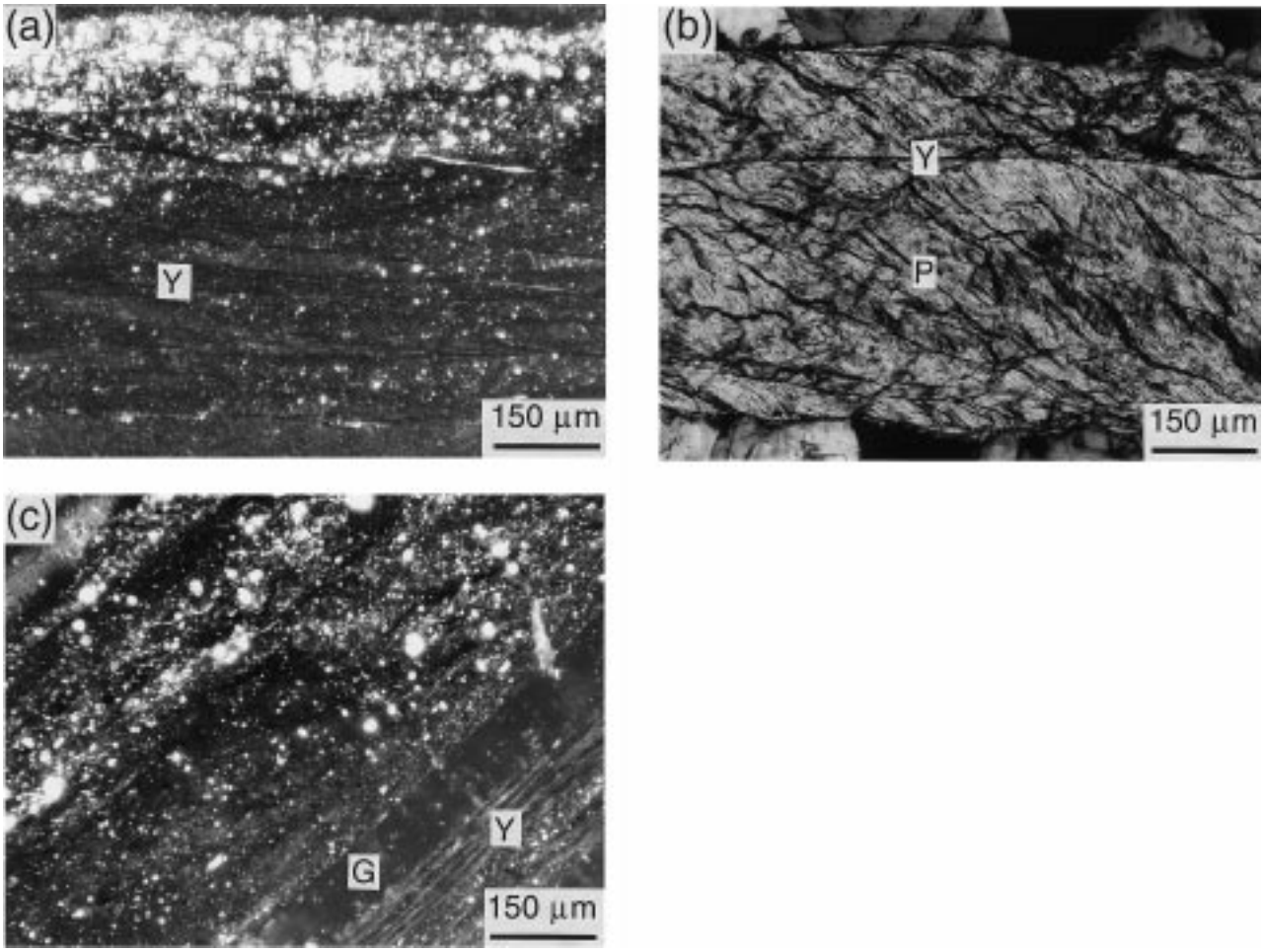

Fig. 5. Microstructures of sheared gouge materials under optical microscopy. (a) Feldspar gouge sheared to about 150 mm at a normal stress of 100 MPa, note the layered structure and numerous Y-shears (Y) in the fine-grained layer. Shear plane is horizontal and sense of shear is sinistral. (b) Muscovite gouge sheared to about 100 mm at a normal stress of 100 MPa. Preferred shape fabric, P-shears (P) and Y-shears (Y) are present. Shear plane is horizontal and shear sense is sinistral. (c) Granitic gouge sheared to about 150 mm at a normal stress of 100 MPa. Note the specimen was delaminated parallel to Y-shears (marked as G). Y-shears (Y) and foliations defined by biotite and oxide can be clearly seen. Shear plane is SW–NE and sense of shear is counter-clockwise.

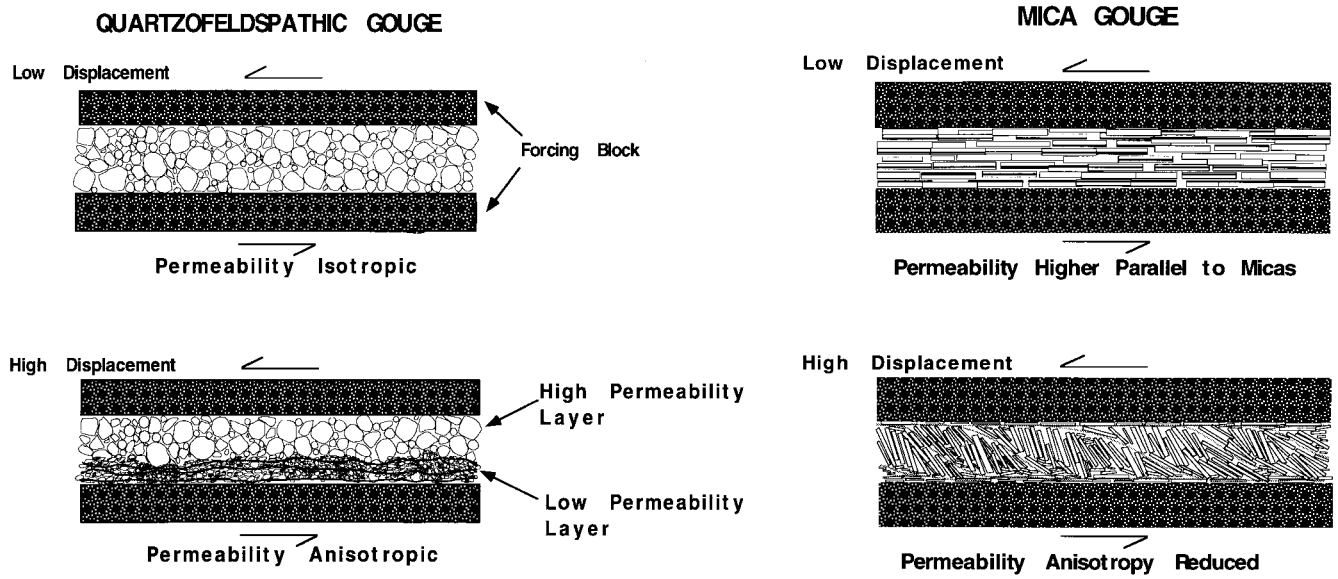

Fig. 6. Schematic diagrams illustrating the development of shear textures in quartzo-feldspathic and mica gouges and the effect on permeability anisotropy.

effective normal stress as shown in Fig. 4(c) and (d). Measurements of pressure dependency of permeability in pure feldspar gouge sheared to 150 mm shows a nonlinear relationship similar to granitic gouge.

It is clear that in quartz and granitic gouges, the value of γ decreases with initial shear sliding up to 15–50 mm, and it increases with further shear sliding (Fig. 4 and Table 2). For example, in quartz gouge, γ is about 0.01417 MPa^{-1} before shear deformation, it decreases to about 0.00625 MPa^{-1} after 15 mm shear sliding and then increases to about 0.02919 MPa^{-1} after about 150 mm shear slip. In contrast, the value of γ in muscovite gouge decreases continuously with increasing shear displacement up to a shear displacement of 150 mm (Fig. 4b).

We were not able to precisely determine the pressure dependency of permeability of unsheared quartzo-feldspathic gouges for fluid flow perpendicular to the layer because of technical difficulties in measuring small amounts of pore pressure differences (<0.01 MPa) across the thin gouge layer. However, the values of γ for fluid flow perpendicular and parallel to the gouge layer are presumably very similar before shear deformation judging from the fact that the permeabilities in the two directions are similar after pressurization to an effective pressure of 100 MPa. In sheared gouge materials, the pressure dependency of permeability for fluid flow parallel to the gouge layer is systematically higher than perpendicular to it by a factor of 2–3 (Table 2), most likely reflecting anisotropic pore networks.

4. Discussion

4.1. Possible causes for permeability anisotropy

The typical microstructures of sheared gouge materials are shown in Fig. 5. The evolution of the characteristic textures for quartzo–feldspathic gouges and mica gouges is summarized in Fig. 6. As will be discussed below, the possible causes for permeability anisotropy in deformed gouge materials are: (1) heterogeneous grain-size reduction; (2) anisotropic shear fractures; and (3) preferred alignment of clay shape fabrics.

In pure quartz and feldspar gouges, the texture is rather homogeneous after initial pressurization and at the early stage of shear deformation (Fig. 6). Individual Riedel shears cannot be traced clearly. In strongly sheared samples, the prominent feature is layered structure (Fig. 5a). The layered structure is defined by differences in particle sizes and numbers of shear fractures. The layers with very fine particle sizes (sub-micron sized) usually contain a number of continuous sliding surfaces (Y-shears), suggesting that they represent localized, strong deformation bands. In the layers with coarse particles, low-angle Riedel shears can be traced in some locations. Detailed studies on the evolution of shear textures during fault slip suggest that the layers with coarse particles represent the remnant of the early stage of shear deformation (Scruggs and Tullis, 1995). The permeability of the layers with fine particle sizes should be relatively lower

because of small pore size and large tortuosity of pore networks. Thus, we conclude that the observed permeability anisotropy in quartz and feldspar gouge materials is mainly due to (1) impediment of fluid flow in the direction perpendicular to the experimental fault by the fine-grained layers and (2) enhancement of fluid flow with Y-shears in the direction parallel to the fault.

In muscovite gouge, the basal planes of mica grains were aligned parallel to the fault plane due to initial packing and pressurization (Fig. 6). Because fluid flow paths perpendicular to the fault plane are much more tortuous than parallel to it, the fluid permeability perpendicular to the fault plane is lower than parallel to it. In sheared muscovite gouge (Fig. 5b), shear deformation took place more uniformly across the whole gouge layer, and there is no layered structure of different particle sizes. The permeability reduction during shear deformation was most likely caused by reducing void spaces between ends of individual mica flakes (Fig. 6). The basal planes of muscovite grains rotated to high angles (about 30–60°) to the fault plane. Some irregularly, but generally widely spaced P-shears and Y-shears were developed between flake surfaces (Fig. 5b). Clearly shear deformation reduced the tortuosity contrast between intergranular fluid flow paths perpendicular and parallel to the fault. The observed permeability anisotropy of about half an order of magnitude for the sheared muscovite gouge probably resulted from anisotropic enhancement of fluid flow by P-shears and Y-shears.

In sheared granitic gouges (Fig. 5c), we observed layered structures similar to those in pure quartz and feldspar gouges. However, there are two distinctive features in granitic gouge: first, within the layer of fine particle sizes, some foliated materials of optically invisible particle sizes are found to be along the sliding (Y-shears) surfaces; and second, within the less deformed layer, there is a low angle ($<20°$) foliation defined by the elongation of mica. These two features would effectively reduce permeability more in the direction perpendicular to the fault, leading to the relatively larger permeability anisotropy in granitic gouge than in pure quartz and feldspar gouges.

4.2. Evolution of pore networks during shear deformation

The equivalent channel model and percolation theory predict that the pressure effect on permeability results from elastic closure, loss of pore connectivity, and pore surface roughness (Walsh, 1981; Walsh and Brace, 1984; Gavrilenko and Gueguen, 1989). The elastic deformation of pores changes fluid permeability by changing the cross-sectional flow area of flow passages. The apertures of long and thin cracks are much more sensitive to pressure than those of equal-dimensioned pores. Thus, in general, rocks with abundant cracks would tend to have higher pressure dependency of permeability. In the present study, we found that the changes in pressure dependency of permeability with shear displacement are rather different between quartzo-feldspathic gouges and mica gouges. We conclude that differences in evolution of the pore network during deformation in quartzo-feldspathic gouges vs mica gouge explains the variations in pressure dependency of permeability.

In sheared gouge materials, porosity is composed of both intergranular pores and shear fractures. At early stages of shear deformation in quartzo-feldspathic materials, severe pore collapse and grain crushing occurred, which resulted in a sharp decrease in intergranular porosity (Fig. 2a). The observed decreases in the pressure dependency of permeability at this stage of deformation indicate that the connected pore network consists mainly of intergranular pores, although some Riedel shears are present. With further shearing, strong grain crushing and reduction in intergranular pores continued in the vicinity of localized shear bands. The presence of multiple, continuous Y-shears suggests the processes of shear band hardening and growth (Beeler et al., 1996), which eliminates most of the intergranular pores. The increases in the pressure dependency of permeability in strongly sheared gouge material indicate that shear fractures, particularly Y-shears, control the pore network and fluid flow. It is unclear at this stage what causes the nonlinear relationship between log permeability and effective normal stress in granitic gouges (Fig. 4).

In muscovite gouge, the early stage compaction is largely due to rearrangement of packing and reduction of pore spaces between mica flakes, grain crushing appears to be minimal. Similar to quartzo-feldspathic gouges, the pressure dependency of permeability decreased due to reduction of the intergranular pores. However, the trend of decreasing pressure dependency of permeability with increasing shear displacement continued up to a shear displacement of 100 mm. This is probably due to first, the difficulties of completely eliminating intergranular pores because of minimum grain crushing and rotation of mica shape fabrics to high angle to the shear direction; and second, to the relatively more homogeneous deformation.

4.3. Comparison with previous studies

4.3.1. Shear slip and permeability

The present studies show that shear sliding generally reduces fluid permeabilities in all gouge materials, with larger reductions in granular materials than in mica gouges. The observation is consistent with triaxial sliding experiments by Morrow et al. (1984) on a number

of natural fault gouges and synthetic clay gouges. Morrow et al. (1984) concluded that the permeability reduction during shear sliding depends on the degree of grain crushing; thus, granular gouges tend to show larger permeability reduction with shear sliding. Hydrostatic compression of a number of porous sandstones also indicates that drastic permeability reductions are associated with the onset of grain crushing at pressures above a critical value (Zhang et al., 1990; Menéndez et al., 1996; Zhu and Wong, 1997).

4.3.2. Anisotropy of permeability

Our large displacement shearing of quartzo-feldspathic gouges demonstrates that the development of permeability anisotropy in reference to the shear plane is largely caused by localization of deformation along Y-shears. Riedel shears, which developed at an early stage of shear sliding, do not appear to play a major role in permeability anisotropy. Permeability anisotropy was previously measured for porous sandstones subjected to a nonhydrostatic stress field (Zoback and Byerlee, 1976; Bruno, 1994; Zhu et al., 1997). In these studies, the fluid permeabilities parallel to the maximum principal (compressive) stress σ_1 and to the least principal stress σ_3 were measured in conventional triaxial compression and extension tests, respectively. Comparisons at the same effective mean stress and porosity level show that permeability parallel to σ_1 is usually one to two orders of magnitude higher than parallel to σ_3, possibly due to preferential alignment of microcracks parallel to σ_1 (Zhu et al., 1997). Our results and these previous studies clearly demonstrate that deviatoric stress is the prerequisite for the development of permeability anisotropy in quartzo-feldspathic materials and that the pattern of anisotropy depends on the deformation geometry.

It is well known that preferred alignment of clay particles may lead to anisotropy of permeability. However, there is a considerable debate about the magnitude of permeability anisotropy (Arch and Maltman, 1990; Brown and Moore, 1993; Brown et al., 1994). Arch and Maltman (1990) conducted uniaxial compression tests on clay-rich wet sediment. They then measured permeability parallel and perpendicular to a slice of the deformed specimen which contained shear zones. They found that permeability parallel to the shear zone is more than two orders of magnitude higher than in the direction perpendicular to the shear zone. In-situ measurements of clays and silty clays during triaxial frictional sliding (Brown and Moore, 1993) and rotary shearing (Brown et al., 1994; Dewhurst et al., 1996a, b) at high effective normal stress show that permeability anisotropy is only about one order of magnitude. Our results on mica gouge support the work of Brown and Moore (1993) and Brown et al. (1994) on wet sediments. The high permeability anisotropy in Arch and Maltman's experiments may be due to the preferential opening of cracks during preparation of their sample slices and during permeability measurements at atmospheric pressure.

4.3.3. Pressure dependency of permeability

Most previous measurements of pressure dependency of permeability were performed on undeformed rocks subject to hydrostatic loading path. Our study presents a first set of data showing the evolution of pressure dependency of permeability with shear deformation. As mentioned in previous sections, the permeabilities in our study were measured under nonhydrostatic conditions with a fixed ratio of about 25:21 between the effective normal stress (effective pressure plus axial stress) and the lateral stress (effective pressure). A direct comparison of our data measured under nonhydrostatic conditions with those data measured under hydrostatic conditions is valid because the axial stress used in our experiments (4–16 MPa) is too low to cause any texture changes such as grain crushing in addition to the hydrostatic pressure-induced elastic closure of pores.

Typical values of pressure dependency of permeability (γ) for different rocks were summarized by David et al. (1994). In porous sandstones and granular gouge materials, the value of γ ranges from 0.001 to 0.02 MPa^{-1}. For clay gouges and low porosity crystalline rocks, the value of γ is higher, usually about 0.01–0.1 MPa^{-1}. Our study shows that the value of γ changes with increasing shear displacement. At the beginning of shear deformation, muscovite gouge has a higher value of γ than quartzo-feldspathic gouges. After a few tens of mm of shear sliding, the differences between different gouges are small. Judging from the trend of the evolution of γ with shear displacement, it appears that at large displacements, quartzo-feldspathic gouge materials would have a much higher value of γ than muscovite gouges. The pressure dependency of permeability in strongly sheared quartzo-feldspathic gouge falls into the range of values for low porosity, microcrack-dominant crystalline rocks.

The value of γ for quartzo-feldspathic gouge sheared to large displacement is close to those determined for natural fault core and damaged zone by Evans et al. (1997). Evans et al. (1997) conducted permeability measurements on core samples representing the three distinctive components (granitic protolith, damaged zone, and gouge zone) of an exhumed fault. They showed that at an effective pressure of 4 MPa, the permeability of the gouge zone is lower than that of the protolith and the damaged zone respectively by about one and two orders of magnitude. Over a range of effective pressures from 2 to 50 MPa, the pressure

dependency of permeability is about 0.2 MPa^{-1} for the protolith, and about 0.03–0.08 MPa^{-1} for the damaged zone and the gouge zone. It is unclear whether syntectonic or post-tectonic mineral alterations made any contribution toward the decrease of permeability and the pressure dependency of permeability in the gouge zone. The study on natural fault products and our studies on synthetic gouge materials suggest that the typical value of γ for strongly deformed gouge zones is most likely above 0.02 MPa^{-1}.

5. Implications to fluid flow within fault zones

Our frictional sliding experiments shed light on the evolution of hydraulic properties of mature fault zones during strain localization. The hydraulic properties of our synthetic gouge materials sheared to large displacements can be extrapolated to natural fault gouges because of similarities of shear textures and particle size distribution (Logan et al., 1979; Rutter et al., 1986; Sammis and Biegel, 1989). Although our synthetic gouges initially did not have the fractal particle size distribution typical of natural fault gouges (Sammis and Biegel, 1989), they are expected to have evolved to the fractal distribution after the first few millimeters of shear sliding, as clearly demonstrated by Biegel et al. (1989). In our gouge specimens sheared to large displacements, fluid permeability was reduced to about 10^{-17}–10^{-20} m^2. Extrapolation of the data of pressure dependency of permeability listed in Table 2 would show that even under lithostatic fluid pressures, the permeability of most sheared gouge materials would still be well below $10^{-15.5}$ m^2. Thus, our experimental results support the conceptual model of Caine et al. (1996) on the permeability structures of mature fault zones in that the strongly sheared fault core would hinder fluid flow. The results imply that large fluid flux may be mainly transported through the damaged zone of a fault zone. The fact that fault cores usually show a larger extent of chemical alteration than the damaged zones could be largely caused by large reaction surfaces of the fine or even disordered particles of the fault core (e.g. Goddard and Evans, 1995; Barnett et al., 1996).

The present study suggests that fluid permeability parallel to the fault plane in fault cores of natural fault zones could be orders of magnitude higher than perpendicular to the fault plane. The presence of significant permeability anisotropy would effectively focus fluid flow along fault zones. We found that the nature of anisotropy changes with gouge mineral compositions. In quartzo-feldspathic material, permeability anisotropy is caused by the formation of layered structures of different particle sizes due to shear localization along Y-shears. The magnitude of permeability anisotropy in the fault core of natural faults may be higher or lower than our measured anisotropy of 1–1.5 orders of magnitude, depending on the degree of shear localization which is characterized both by the particle size and by the width of the localized zone relative to the less deformed region (Zhang and Tullis, 1998). We measured a permeability anisotropy of about one order of magnitude for muscovite gouge, which probably represents the largest possible anisotropy due to preferred alignment of clay shape fabrics. In sheared muscovite gouge, we noticed that shear deformation took place rather uniformly within the whole gouge layer, without significant grain crushing. If shear deformation does localize, as in biotite and serpentinite gouges (Reinen et al., 1992; Scruggs and Tullis, 1995), the permeability anisotropy is expected to be higher than one order of magnitude. Combined effects of shear localization with clay shape fabrics may lead to extremely high permeability anisotropies where chemical alterations of feldspar into clay minerals take place.

Our experimental results have implications for fluid pressure distribution within fault zones. As clearly demonstrated by Rice (1992) and David et al. (1994), the generation and maintenance of supralithostatic pore pressures within major strike slip faults require that firstly, the permeability of fault zones decreases rapidly with increasing depth (high value of γ) and secondly, there is a steady fluid injection from the ductile root of the fault zone to compensate leaking of fluid into surrounding country rocks. Apparently, to effectively compensate fluid leaking, the fault zone needs to act as a conduit for fluid transport from below and at the same time to act as a barrier to lateral flow into the country rock, which can only be achieved with significantly high permeability anisotropy. Our study shows that compressional and shear deformation can result in significant permeability anisotropy in fault gouge zone. Taking into account the presence of fractured–damaged zones surrounding the gouge zone in many mature fault zones (Teufel, 1987; Smith et al., 1990; Caine et al., 1996), we expect that the permeability anisotropy in many natural fault zones can be sufficiently large to effectively focus fluid flow along fault zones. Our measurement also shows that the value of γ in strongly sheared gouge materials ranges from 0.004 to 0.03 MPa^{-1}. This range of γ value is about one order of magnitude lower than the value (0.2 MPa^{-1}) used in Rice's fault model, suggesting that the development of supralithostatic pore pressure in fault cores would require a larger amount of fluid injection than that predicted by Rice (1992). The differences in the effects of shear strain and pressure on permeability and its anisotropy between quartzo-feldspathic gouges and clay-rich materials could lead to heterogeneous distribution of pore

fluid pressure and thus to the formation of compartments of different fluid pressures as proposed by Byerlee (1993). In clay-rich gouges, the permeability is low and it does not change much as fluid pressure is built up; therefore, high fluid pressure could be built up and trapped for a rather long geological time. In quartzo-feldspathic gouges, the permeability is higher than in clay gouges and it increases substantially with increasing pore fluid pressure, thus, fluid pressure should be lower than in clay-rich gouges. Similarly, because the pressure dependency of permeability varies with strain, fluid pressures within gouge materials of similar compositions would also vary spatially due to localization of strain. Rupture of the walls between compartments of different pore fluid pressures may eventually trigger earthquakes (Byerlee, 1993; Miller et al., 1996).

Acknowledgements

We wish to thank T.-f. Wong and R. Myers for their thorough reviews. Discussions with Jan Tullis and Dick Yund were very helpful. The research was supported by NSF grant EAR-9317038 and USGS grant 1434-94-G-2422 to TET.

References

Anderson, J.L., Osborne, R.H., Palmer, D.F., 1983. Cataclastic rock of the San Gabriel fault, an expression of deformation at deeper crustal levels in the San Andreas fault zone. Tectonophysics 98, 209–251.

Antonellini, M., Aydin, A., 1994. Effect of faulting on fluid flow in porous sandstones: Petrophysical properties. American Association of Petroleum Geologists Bulletin 78, 355–377.

Arch, J., Maltman, A., 1990. Anisotropic permeability and tortuosity in deformed wet sediments. Journal of Geophysical Research 95, 9035–9046.

Barnett, D.E., Bowman, J.R., Bromley, C., Cady, C., 1996. Kinetically limited isotope exchange in a shallow level normal fault, Mineral Mountains, Utah. Journal of Geophysical Research 101, 673–685.

Beeler, N.M., Tullis, T.E., Blanpied, M.L., Weeks, J.D., 1996. Frictional behavior of large displacement experimental faults. Journal of Geophysical Research 101, 8697–8715.

Biegel, R.L., Sammis, C.G., Dieterich, J.H., 1989. The frictional properties of a simulated gouge having a fractal particle distribution. Journal of Structural Geology 11, 827–846.

Brace, W.F., 1980. Permeability of crystalline and argillaceous rocks. International Journal of Rock Mechanics and Mining Sciences 17, 241–251.

Brace, W.F., Orange, A.S., Madden, T.R., 1965. The effect of pressure on the electrical resistivity of water-saturated crystalline rocks. Journal of Geophysical Research 70, 5669–5678.

Brown, K.M., Moore, J.C., 1993. Comment on "anisotropic permeability and tortuosity in deformed wet sediments by J. Arch and A. Maltman". Journal of Geophysical Research 98, 17859–17864.

Brown, K.M., Bekins, B., Clennell, B., Dewhurst, D., Westbrook, G., 1994. Heterogeneous hydrofracture development and accretionary fault dynamics. Geology 22, 259–262.

Bruhn, R.L., Yonkee, W.E., Perry, W.T., 1990. Structural and fluid-chemical properties of seismogenic normal faults. Tectonophysics 175, 139–157.

Bruno, M.S., 1994. Micromechanics of stress-induced permeability, anisotropy and damage in sedimentary rock. Mechanics of Materials 18, 31–48.

Byerlee, J., 1990. Friction, overpressure and fault normal compression. Geophysical Research Letters 17, 2109–2112.

Byerlee, J., 1993. Model for episodic flow of high-pressure water in fault zones before earthquakes. Geology 21, 303–306.

Caine, J.S., Evans, J.P., Forster, C.B., 1996. Fault zone architecture and permeability structure. Geology 24, 1025–1028.

Chester, F.M., Logan, J.M., 1986. Implications for mechanical properties of brittle faults from observations of the Punchbowl fault zone, California. Pure and Applied Geophysics 124, 79–106.

Chester, F.M., Evans, J.P., Biegel, R.L., 1993. Internal structure and weakening mechanisms of the San Andreas fault. Journal of Geophysical Research 98, 771–786.

David, C., Wong, T.-f., Zhu, W., Zhang, J., 1994. Laboratory measurements of compaction-induced permeability change in porous rocks: Implications for the generation and maintenance of pore pressure excess in the crust. Pure and Applied Geophysics 143, 425–456.

Davis, S.N., DeWiest, R.J.M., 1966. Hydrogeology. John Wiley, New York, p. 463.

Dewhurst, D.N., Brown, K.M., Clennell, M.B., Westbrook, G.K., 1996a. A comparison of the fabric and permeability anisotropy of consolidated and sheared silty clay. Engineering Geology 42, 253–267.

Dewhurst, D.N., Clennell, M.B., Brown, K.M., Westbrook, G.K., 1996b. Fabric and hydraulic conductivity of sheared clays. Géotechnique 46, 761–768.

Evans, J.P., Forster, C.B., Goddard, J.V., 1997. Permeability of fault-related rocks, and implications for hydraulic structure of fault zones. Journal of Structural Geology 19, 1393–1404.

Ganser, D.R., 1987. Hydrogeologic characteristics of the Ramapo fault, Northern New Jersey. Ground Water 25, 664–671.

Gavrilenko, P., Gueguen, Y., 1989. Pressure dependency of permeability: A model for crack rocks. Geophysical Journal International 98, 159–172.

Goddard, J.V., Evans, J.P., 1995. Chemical changes and fluid–rock interaction in faults of crystalline thrust sheets, northwestern Wyoming, U.S.A. Journal of Structural Geology 17, 533–547.

Gu, Y., Wong, T.-f., 1994. Development of shear localization in simulated quartz gouge: Effect of cumulative slip and gouge particle size. Pure and Applied Geophysics 143, 387–422.

Hippler, S.J., 1993. Deformation microstructures and diagenesis in sandstone adjacent to an extensional fault: Implications for the flow and entrapment of hydrocarbons. American Association of Petroleum Geologists Bulletin 77, 625–637.

Hubbert, M.K., 1953. Entrapment of hydrocarbon under hydrodynamic conditions. American Association of Petroleum Geologists Bulletin 37, 1954–2026.

Levorsen, A.I., 1967. Geology of Petroleum. W.H. Freemen, San Francisco, California.

Logan, J.M., Friedman, M., Higgs, N., Dengo, C., Shimamoto, T., 1979. In: Experimental studies of simulated gouge and their application to studies of natural fault zones, Open-File Report 79-1239. U.S. Geological Survey, pp. 305–343.

Logan, J.M., Dengo, C.A., Higgs, N.G., Wang, Z.Z., Wong, T.-f., 1992. Fabrics of experimental fault zones: Their development and relationship to mechanical behavior. In: Evans, B. (Ed.), Fault Mechanics and Transport Properties of Rocks. Academic Press, New York, pp. 33–67.

Mandl, G., De Jong, L.N.J., Maltha, A., 1977. Shear zones in granular materials. Rock Mechanics 9, 95–144.

Menéndez, B., Zhu, W., Wong, T.-f., 1996. Micromechanics of brittle faulting and cataclastic flow in Berea sandstone. Journal of Structural Geology 18, 1–16.

Miller, S.A., Nur, A., Olgaard, D.L., 1996. Earthquakes as a coupled shear stress–high pore pressure dynamical system. Geophysical Research Letters 23, 197–200.

Moore, J.C., Vrolijk, P., 1992. Fluids in accretionary prisms. Reviews of Geophysics 30, 113–135.

Morrow, C.A., Shi, L.Q., Byerlee, J.D., 1984. Permeability of fault gouge under confining pressure and shear stress. Journal of Geophysical Research 89, 3193–3200.

Pittman, E.D., 1981. Effect of fault-related granulation on porosity and permeability of quartz sandstones, Simpson group (Ordovician), Oklahoma. American Association of Petroleum Geologists Bulletin 65, 2381–2387.

Powley, D.E., 1990. Pressure and hydrogeology in petroleum basins. Earth Science Reviews 29, 215–226.

Reinen, L.A., Tullis, T.E., Weeks, J.D., 1992. Two-mechanisms model for frictional sliding of serpentinite. Geophysical Research Letters 19, 1535–1538.

Rice, J.R., 1992. Fault stress states, pore pressure distributions, and the weakness of the San Andreas fault. In: Evans, B., Wong, T.-f. (Eds.), Earthquake Mechanics and Transport Properties of Rocks. Academic Press, London, pp. 475–503.

Rutter, E.H., Maddock, R.H., Hall, S.H., White, S.H., 1986. Experimental study of microstructural evolution and mechanical properties of synthetic and natural fault gouge. Pure and Applied Geophysics 124, 3–30.

Sammis, C.G., Biegel, R.L., 1989. Fractals, fault-gouge, and friction. Pure and Applied Geophysics 131, 255–271.

Scholz, C.H., Anders, M.H., 1994. The permeability of faults, in the mechanical involvement of fluids in faulting, Open-File Report 94-228. U.S. Geological Survey, pp. 247–253.

Scruggs, V.J., Tullis, T.E., 1995. Localization and mechanical behavior correlation in the frictional deformation of feldspar and mica gouges. EOS Transactions American Geophysical Union 76, 560.

Seeburger, D.A., 1981. Studies of natural fractures, fault zone permeability, and a pore space–permeability model. PhD thesis, Stanford University, University Microfilms International.

Sibson, R.H., 1977. Fault rocks and fault mechanisms. Geological Society of London Journal 133, 191–231.

Sibson, R.H., 1981. Fluid flow accompanying faulting: Field evidence and models. In: Simpson, D.W., Richards, P.G. (Eds.), Earthquake Prediction—An International Review, Monograph, Maurice Ewing Series 4. American Geophysical Union, pp. 593–603.

Sleep, N.H., Blanpied, M.L., 1992. Creep, compaction, and the weak rheology of major faults. Nature 359, 687–692.

Smith, D.A., 1966. Theoretical considerations of sealing and nonsealing faults. American Association of Petroleum Geologists Bulletin 50, 363–374.

Smith, D.A., 1980. Sealing and nonsealing faults in Gulf Coast Salt Basin. American Association of Petroleum Geologists Bulletin 64, 145–172.

Smith, L., Forster, C., Evans, J., 1990. Interaction of fault zones, fluid flow, and heat transfer at the basin scale. In: Neuman, S.P., Neretnieks, I. (Eds.), Hydrogeology of Low Permeability Environments. Verlag Heinz Heise, Hannover, Germany, pp. 41–67.

Teufel, L., 1987. Permeability changes during shear deformation of fractured rock. In: Farman, I.W., Daemen, J., Desai, C.S., Glass, C.E., Neuman, S.P. (Eds.), Proceedings of 28th US Symposium on Rock Mechanics. A.A.Balkema Publishers, Brookfield, USA, pp. 473–480.

Tullis, T.E., Weeks, J.D., 1986. Constitutive behavior and stability of frictional sliding of granite. Pure and Applied Geophysics 124, 384–414.

Walsh, J.B., 1981. Effect of pore pressure and confining pressure on fracture permeability. International Journal of Rock Mechanics and Mining Sciences 18, 429–435.

Walsh, J.B., Brace, W.F., 1984. The effect of pressure on porosity and the transport properties of rock. Journal of Geophysical Research 89, 9425–9431.

Zhang, J., Wong, T.-f., Davis, D.M., 1990. Micromechanics of pressure-induced grain crushing in porous rocks. Journal of Geophysical Research 95, 341–352.

Zhang, S., Tullis, T.E., 1998. The effect of fault slip on permeability and permeability anisotropy in an artificial quartz gouge. Tectonophysics 295, 41–52.

Zhu, W., Wong, T.-f., 1997. The transition from brittle faulting to cataclastic flow: Permeability evolution. Journal of Geophysical Research 102, 3027–3041.

Zhu, W., Montesi, L.G., Wong, T.-f., 1997. Shear-enhanced compaction and permeability reduction: Triaxial extension tests on porous sandstone. Mechanics of Materials 25, 199–214.

Zoback, M.D., Byerlee, J.D., 1976. Effect of high-pressure deformation on permeability of Ottawa sand. American Association of Petroleum Geologists Bulletin 60, 1531–1542.